MODELING PERFORMANCE OF THREE-DIMENSIONAL NANOJUNCTION PHOTOVOLTAIC DEVICES

Artit Wangperawong[1] and Stacey F. Bent[2]
[1]Department of Electrical Engineering, Stanford University, Stanford, CA, United States
[2]Department of Chemical Engineering, Stanford University, Stanford, CA, United States

ABSTRACT

We present an analytical approach for modeling the device physics of three-dimensionally nanostructured devices. The approach for the first time describes three-dimensional diffusion as well as distinguishes between isolated and interdigitated pn junction devices. The modeling technique can be applied to various device architectures, including isolated radial pn junctions, inverted grain boundary junctions, point-contact nanojunctions, and extended nanojunctions. As a test case, we use low quality material properties of CdTe to show that the solar power conversion efficiencies of the nanojunction designs are superior to that of the planar junction, with the extended nanojunction geometry performing the best.

INTRODUCTION

One of the major motivations for studying nanostructured solar cells has been enhanced charge collection [1,9]. Despite increasing experimental work in three-dimensionally (3D) nanostructured device structures for solar cells [2-6], theoretical treatment of charge carrier diffusion and collection in 3D has been limited. In 3D interdigitated geometries, photogenerated carriers within a unit cell can diffuse to any one of the nearby junctions, not just the junction in the unit cell. A complete analysis should include this effect, as reducing the charge collection distance is a major advantage of nanostructures.

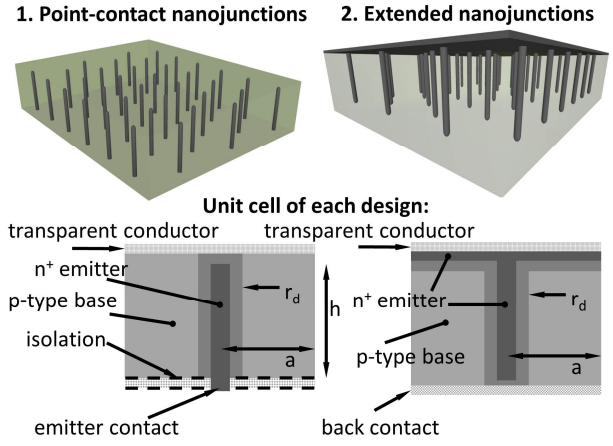

Figure 1. Two examples of 3D interdigitated nanoarchitectures modeled.

Existing theoretical studies on 3D geometries have cylindrically integrated two-dimensional numerical simulations [7,8], imposing unit cell boundary conditions which do not represent an interdigitated device. Additionally, such an approach may not accommodate photogeneration profiles which are not cylindrically symmetric or completely asymmetric profiles. Full 3D analysis has not been practical numerically due to the computational resources required. To address these issues, we recently introduced an analytical approach for studying 3D nanoarchitectures that can be broadly applied to both isolated and interdigitated geometries of various forms [9]. Two of the designs we considered are shown in Fig. 1. Here we discuss in more detail the modeling and performance of 3D nanojunction solar cells.

METHOD

The minority carrier diffusion and collection properties can be calculated by first considering the charge collection probability, φ . By definition, φ is the fraction of photogenerated minority carriers at a point within the device which diffuse to a depletion edge and contribute to photocurrent [10]. According to the reciprocity theorem [11], the duality between dark carrier distribution and photogenerated carrier collection implies that φ obeys its own diffusion equation,

$$\frac{1}{r}\frac{\partial}{\partial r}\left(r\frac{\partial \varphi_m}{\partial r}\right)+\frac{\partial^2 \varphi_m}{\partial z^2}-\frac{1}{L_m^{\,2}}\varphi_m=0 \quad m=1,2, \qquad (1)$$

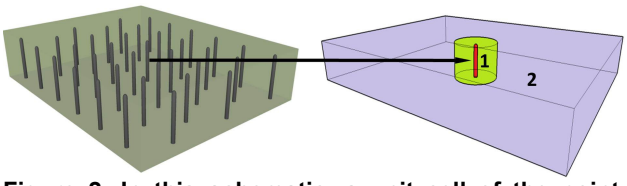

Figure 2. In this schematic, a unit cell of the point-contact geometry is shown to perceive the rest of the unit cells as a homogenous and isotropic medium surrounding it.

where φ_1 is the solution within the unit cell, and φ_2 is the solution outside. The two solutions are necessary for the effective medium approximation to be described below. Exploiting the duality is a powerful technique to simplify complicated calculations, especially since the reciprocity

theorem applies to arbitrary 3D geometries with arbitrary doping profiles and variable band gap, including abrupt compositional changes, grain boundaries and floating junctions [12].

Using an effective medium approximation for the minority carrier diffusion in the base [13], we can model the effect of neighboring junctions on charge carriers within each 3D unit cell **1** of an interdigitated geometry (Fig. 2). The diffusion-collection equation can be analytically solved in cylindrical coordinates by abstracting away the rest of the unit cells **2**. From the perspective of a unit cell **1**, the boundary conditions are determined by the average effect of the rest of the unit cells **2** of the device in which it is embedded. Unit cell **1** has a minority carrier diffusion length of L_1 and interacts with a medium **2** with an effective minority carrier diffusion length L_2. L_1 can be used to calculate L_2 by self-consistent averaging, since the foregoing argument applies to each and every unit cell of the device.

Following such analysis, the boundary conditions between **1** and **2** due to continuity are generally

$$\varphi_1(r=a)=\varphi_2(r=a) \tag{2}$$

$$\left.\frac{\partial\varphi_1}{\partial r}\right|_{r=a}=\left.\frac{\partial\varphi_2}{\partial r}\right|_{r=a}, \tag{3}$$

and the boundary condition at depletion edges is

$$\left.\varphi_1\right|_{depletion}=1. \tag{4}$$

The remaining boundary conditions depend on the specific device geometry and surface assumptions made. Eqn. 1 reduces to an ordinary differential equation for the point-contact nanojunction geometry assuming perfectly selective contacts on the front and back surfaces. The solutions φ_1 and φ_2 then involve the zeroth order modified Bessel functions. For the extended nanojunction design, a special transformation is necessary to obtain an ordinary differential equation.

Next we apply the definition of effective diffusion length [14], equating the photocurrent of the nanostructured cell under uniform photogeneration rate G_0 to that of a hypothetical homogenous and isotropic material with minority carrier diffusion length, L_e:

$$\int_V G_0\varphi_{planar}\,dV=\sum_i^N\left\{\int_{r_{j,i}}^{a_i}\int_0^h G_0\varphi_1\,dz\,2\pi r\,dr\right\} \tag{5}$$

where $r_{j,i}$ is the position of the metallurgical junction of the ith unit cell of the N total unit cells comprising the device, h is the thickness of the cell, and

$$\varphi_{planar}(z)=\frac{\cosh\left((h-z)/L_e\right)}{\cosh\left(h/L_e\right)} \tag{6}$$

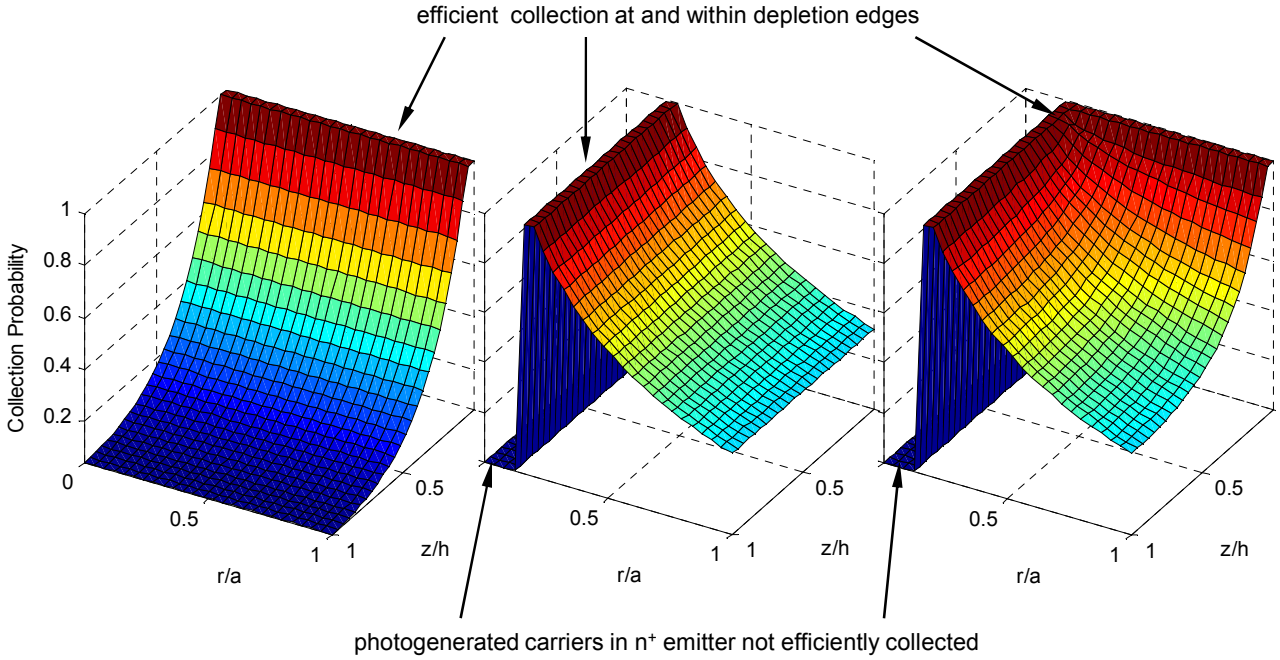

Figure 3. Examples of collection probability distributions φ_1 plotted for planar, point-contact and extended device architectures respectively left to right.

when the bottom contact is perfectly selective. We can thus solve for L_2 using L_1 by recognizing that for consistency all N unit cells are equivalent and that L_2 is equal to L_e. With L_2 known, φ for the entire device is determined (Fig. 3).

For the isolate radial pn junctions, the right-hand side of Eqn. 2 is simply surface recombination. The effective medium approximation is unnecessary because it is not an interdigitated structure. For the inverted grain boundary junctions,

$$\left.\frac{\partial \varphi_1}{\partial r}\right|_{r=0} = 0\,, \tag{7}$$

due to symmetry at the center axis, assuming columnar cylindrical grains.

Using φ_1, in all cases we again invoke the reciprocity theorem to calculate the ideal dark current and depletion region recombination current. The two together normalized to the illumination area is typically referred to as the *dark current* of a solar cell. The depletion region recombination current, also known as the space charge recombination current, can be calculated by linearizing the potential across the depletion region.

The photocurrent can be calculated by integrating the product of φ_1 and the photogeneration profile across the entire device. The photogeneration profile need not be symmetric in any way and can be obtained from either full-field optical solutions or geometric optics, depending on the length scale of the device structures and the degree of accuracy required. To obtain the overall J-V curves (Fig. 4), we superimpose the various current contributions as a function of applied voltage. To obtain IQE and EQE curves (not shown), the same calculation for photocurrent can be used as a function of wavelength.

RESULTS AND DISCUSSION

Shown in Fig. 3 are example solutions of φ_1 for the planar, point-contact and extended device architectures. We have assumed for this analysis that any photogeneration in the heavily doped n^+ emitter does not contribute to photocurrent. This is the reason why $\varphi_1 = 0$ for $r < r_j$ in the nanojunction cases. For the horizontal junctions, $\varphi_1 = 0$ in the emitters is not shown but is accounted for in producing Fig. 3. φ_1 is greatest around the depletion edges, implying that for maximum photocurrent the vertical nanojunctions should be placed as close to each other as possible. Moreover, among the designs modeled the extended architecture has the highest collection probability throughout the device. This is the reason that for low-quality CdTe where collection is diffusion limited, the extended device outperforms the point-contact one in terms of short-circuit current, fill-factor and efficiency (Fig. 4).

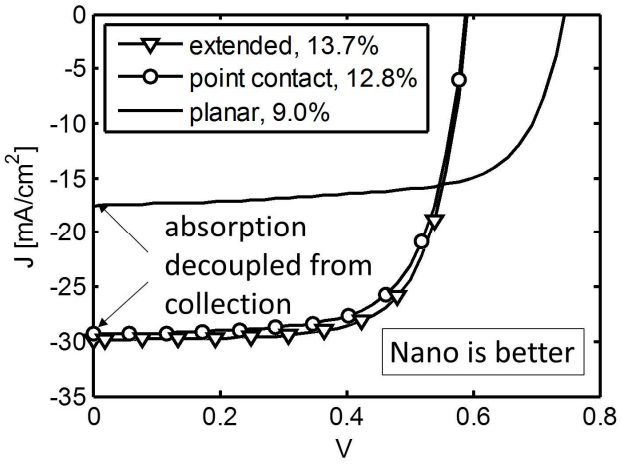

Figure 4. Optimized performance of planar, point-contact nanojunction and extended nanojunction solar cell devices under AM 1.5G illumination. All material properties are equal among the devices. Inset: Legend with corresponding energy conversion efficiencies.

In order to calculate quantitative values for the J-V curves shown in Fig. 4, we have used material properties of CdS and low-quality CdTe [9]. Low-quality entails higher doping due to the higher number of defects, which lowers mobility and diffusion length.

Unlike in high-quality planar CdTe, photogenerated electrons beyond the depletion region in the low-quality planar case cannot get collected because the minority carrier diffusion length is not long enough. Therefore vertical nanojunctions are beneficial in decoupling absorption from carrier collection. This effect is apparent in the difference in short-circuit current between planar and nanojunction devices. The tradeoff made to maintain high short-circuit current is the loss in open-circuit voltage, which is caused by the higher junction interfacial area giving rise to dark current. Nevertheless, an overall benefit in energy conversion efficiency is predicted for the nanojunction devices. Compared to other nanojunction device models accounting for radial variation [1], the nanojunction efficiency advantage here over the planar device does not rely on operating in full depletion nor assume a higher lifetime in the depletion region than that of the quasineutral region.

CONCLUSION

Recently there have been many new experimental device architectures utilizing vertical nanojunctions to decouple light absorption from charge carrier collection. Two new

solar cell device architectures utilizing vertical nanojunctions are presented—the point-contact and the extended geometries—as well as the isolated radial and inverted grain boundary geometries. Despite great experimental work in the field, theoretical studies have been limited. We have developed models that for the first time describe the device performance of nanostructured solar cells in 3D, distinguishing between isolated and interdigitated nanojunctions. Our analytical approach is a powerful tool for designing nanostructured solar cells of various architectures and materials. Given ongoing efforts worldwide to experimentally demonstrate efficient nanostructured devices, these results have important implications for proper design of high-performing solar cells made of inexpensive and low-quality materials.

ACKNOWLEDGEMENTS

Studies were carried out as part of the Center on Nanostructuring for Efficient Energy Conversion, an EFRC funded by the U.S. Department of Energy, Office of Basic Energy Sciences under Award No. DE-SC0001060. A.W. acknowledges financial support from the DOE, Office of Science Graduate Fellowship Program, made possible in part by the American Recovery and Reinvestment Act of 2009, administered by ORISE-ORAU under Contract No. DE-AC05-06OR23100, and support from National Science Foundation under Grant No. CBET 0930098.

REFERENCES

[1] B.M. Kayes, H.A. Atwater and N.S. Lewis, “Comparison of the device physics principles of planar and radial p-n junction nanorod solar cells”, *J. Appl. Phys*. **97**, 2005, pp. 114302.

[2] Z. Fan et al., "Three-dimensional nanopillar-array photovoltaics on low-cost and flexible substrates", *Nature Mater.* **8**, 2009, pp. 648-653.

[3] K.-Q. Peng et al., "High-Performance Silicon Nanohole Solar Cells“, *J. Am. Chem. Soc*. **20**, 2010, pp. 6872-6873.

[4] M. C. Putnam at al., “Si microwire-array solar cells”, *Energy Environ. Sci*. **3**, 2010, pp. 1037-1041.

[5] E. C. Garnett and P. D. Yang, “Silicon Nanowire Radial p−n Junction Solar Cells”, *J. Am. Chem. Soc*. **130**, 2008, pp. 9224-9225.

[6] B. Tian et al., “Coaxial silicon nanowires as solar cells and nanoelectronic power sources”, *Nature* **449**, 2007, pp. 885-889.

[7] M. D. Kelzenberg et al., “Predicted Efficiency of Si Wire Array Solar Cells”, *34th IEEE PVSC*, 2009, pp. 1948-1953.

[8] R. Kapadia, Z. Fan and A. Javey, “Design constraints and guidelines for CdS/CdTe nanopillar based photovoltaics”, *Appl. Phys. Lett*. **96**, 2010, pp. 103116.

[9] A. Wangperawong and S. F. Bent, “Three-dimensional nanojunction device models for photovoltaics”, *Appl. Phys. Lett*. **98**, 2011, pp. 233106.

[10] M. A. Green, *Solar Cells: Operating Principles, Technology, and System Applications* (Prentice-Hall, New Jersey, 1982).

[11] C. Donolato, “A reciprocity theorem for charge collection”, *Appl. Phys. Lett*. **46**, 1985, pp. 270.

[12] M. A. Green, “Generalized relationship between dark carrier distribution and photocarrier collection in solar cells”, *J. App. Phys*. **81**, 1997, pp. 268-271.

[13] C. Donolato, “Voronoi network modelling of multicrystalline silicon solar cells”, *Semicond. Sci. Technol*. **15**, 2000, pp. 15-23.

[14] C. Donolato, “Effective diffusion length of multicrystalline solar cells”, *Semicond. Sci. Technol.*, **13**, 1998, pp. 781-787.